

Evaluation of zinc-doped mesoporous hydroxyapatite microspheres for the construction of a novel biomimetic scaffold optimized for bone augmentation

Weilin Yu,^{1,*} Tuan-Wei Sun,^{2,3,*} Chao Qi,^{2,3} Zhenyu Ding,¹ Huakun Zhao,¹ Shichang Zhao,¹ Zhongmin Shi,¹ Ying-Jie Zhu,^{2,3} Daoyun Chen,¹ Yaohua He^{1,4}

¹Department of Orthopedics, Shanghai Jiao Tong University Affiliated Sixth People's Hospital, ²State Key Laboratory of High Performance Ceramics and Superfine Microstructure, Shanghai Institute of Ceramics, Chinese Academy of Sciences, Shanghai, ³University of Chinese Academy of Sciences, Beijing, ⁴School of Biomedical Engineering, Shanghai Jiao Tong University Affiliated Sixth People's Hospital, Shanghai, China

*These authors contributed equally to this work

Correspondence: Yaohua He
Department of Orthopedics, Shanghai Jiao Tong University Affiliated Sixth People's Hospital, 600 Yishan Road, Shanghai 200233, China
Tel +86 21 2405 8037
Email hyhua18930177339@163.com

Ying-Jie Zhu
State Key Laboratory of High Performance Ceramics and Superfine Microstructure, Shanghai Institute of Ceramics, Chinese Academy of Sciences, 1295 Dingxi Road, Shanghai 200050, China
Tel +86 21 5241 2616
Email y.j.zhu@mail.sic.ac.cn

Abstract: Biomaterials with high osteogenic activity are desirable for sufficient healing of bone defects resulting from trauma, tumor, infection, and congenital abnormalities. Synthetic materials mimicking the structure and composition of human trabecular bone are of considerable potential in bone augmentation. In the present study, a zinc (Zn)-doped mesoporous hydroxyapatite microspheres (Zn-MHMs)/collagen scaffold (Zn-MHMs/Coll) was developed through a lyophilization fabrication process and designed to mimic the trabecular bone. The Zn-MHMs were synthesized through a microwave-hydrothermal method by using creatine phosphate as an organic phosphorus source. Zn-MHMs that consist of hydroxyapatite nanosheets showed relatively uniform spherical morphology, mesoporous hollow structure, high specific surface area, and homogeneous Zn distribution. They were additionally investigated as a drug nanocarrier, which was efficient in drug delivery and presented a pH-responsive drug release behavior. Furthermore, they were incorporated into the collagen matrix to construct a biomimetic scaffold optimized for bone tissue regeneration. The Zn-MHMs/Coll scaffolds showed an interconnected pore structure in the range of 100–300 μm and a sustained release of Zn ions. More importantly, the Zn-MHMs/Coll scaffolds could enhance the osteogenic differentiation of rat bone marrow-derived mesenchymal stem cells. Finally, the bone defect repair results of critical-sized femoral condyle defect rat model demonstrated that the Zn-MHMs/Coll scaffolds could enhance bone regeneration compared with the Coll or MHMs/Coll scaffolds. The results suggest that the biomimetic Zn-MHMs/Coll scaffolds may be of enormous potential in bone repair and regeneration.

Keywords: drug delivery, mesoporous hydroxyapatite microspheres, zinc, biomimicry, scaffold, bone regeneration

Introduction

Despite rapid developments in biotechnology and biomaterials, reconstruction of critical-sized bone defects resulting from tumor, infection, trauma, and congenital skeletal abnormalities remains a great challenge.^{1–3} For better restoration of large bone defects, bone tissue engineering scaffolds with both excellent osteoconductivity and osteoinductivity are desirable. Ideally, the scaffolds should not only act as physical template for the guidance of new bone ingrowth but also offer a stimulatory microenvironment to direct cellular differentiation. Autologous trabecular bone is widely regarded as the gold standard for bone defect repair. It serves as an ideal scaffold that provides not only growth factors and cells but also mechanical support after implantation

into the defects.^{4,5} However, problems associated with its use include tissue availability, donor morbidity, and high care cost.⁵ Hence, the development of biomimetic scaffolds resembling the composition and structure of autologous bone is hopeful to overcome these limitations.

So far, biomimicry has been demonstrated to be a powerful strategy to develop bone tissue engineering scaffolds that could sustain cellular proliferation, differentiation, and functionality similar to those normally occurring in living organisms.^{6,7} The hydroxyapatite/collagen composite scaffolds mimicking the structure and composition of trabecular bone were extensively investigated, and they have been shown to have great potential in bone repair and regeneration.⁸⁻¹⁰ The hydroxyapatite–collagen pairing naturally occurs in bone, whereby the collagen matrix provides strength and structural stability, whereas hydroxyapatite reinforces the organic matrix.¹¹ The organic matrix containing collagen and noncollagenous proteins plays an important role in mineralization, during which the organic matrix not only directs mineral deposition but also guides its growth.^{12,13} The hydroxyapatite/collagen composite scaffolds mimicking the composition of trabecular bone have been demonstrated to be biocompatible, biodegradable, osteoconductive, and osteoinductive in previous studies.^{11,14} However, compared with the hydroxyapatite/collagen composite scaffolds, the hydroxyapatite within human bone is characterized by a multitude of doping elements that substitute either phosphate or calcium in the crystal lattice. The apatite mineral in human bone mainly consists of non-stoichiometric apatite crystals, and CO_3^{2-} is one of the most abundant doping ions.¹⁵ Bone mineral also contains a series of trace elements such as zinc, magnesium, strontium, silica, and manganese.¹⁶ Although they represent only a small fraction of mineral, they play a crucial role in bone metabolism.¹⁷ Inspired by the idea that hydroxyapatite/collagen composite scaffolds mimic bone mineral chemistry and that trace elements regulate bone metabolism, the introduction of trace elements into hydroxyapatite/collagen composite scaffolds can theoretically improve their osteoinductive potential.

One of essential trace elements Zn plays an important role in the development and normal growth of skeletal system. Approximately 30% of total Zn in the body is stored in the bone tissue. Zn deficiency impairs the development of skeletal system and associates with the pathogenesis of osteoporosis.^{18,19} It is well accepted that Zn can stimulate bone formation and enhance osteogenic response in osteoblasts by increasing cell proliferation, osteogenesis-related gene expression, and extracellular matrix synthesis.²⁰⁻²² Therefore, Zn has been

introduced into various biomaterials with a view to improve their bone-forming ability. Indeed, Zn-incorporated bioactive glasses,²³ coatings,^{24,25} and calcium phosphate (CaP)²⁶ showed enhanced osteoinductive potential. However, the development of Zn-incorporated hydroxyapatite/collagen composite scaffolds has not yet been reported, and the effects of Zn on the biological responses of the composite scaffolds remain to be investigated.

CaP such as hydroxyapatite, as the main component of bone mineral, is widely used for the construction of biomimetic bone tissue engineering scaffolds. Among the CaP-based materials, nanostructured CaP porous microspheres attract increasing attention because of their high specific surface area and three-dimensional (3D) hierarchical structure, which make them favorable in the applications of drug delivery and tissue engineering. Recently, a series of nanostructured CaP porous microspheres has been developed in our laboratory through a microwave-hydrothermal method by using different organic phosphorus sources.²⁷⁻²⁹ These CaP porous microspheres were efficient in drug delivery because of their hierarchically porous nanostructure and high specific surface area. Compared with the CaP particles with a relatively large size ($>10\ \mu\text{m}$) and the monoblock CaP bioceramic scaffolds, the nanostructured CaP microspheres with a smaller size ($\sim 1\ \mu\text{m}$) and a relatively high specific surface area are easier to degrade.¹¹ Moreover, the nanostructured CaP porous microspheres have a much larger surface area to volume ratio, and consequently, a composite scaffold may exhibit improved mechanical properties arising from strong interactions at interfaces. In view of these advantages, the nanostructured CaP porous microspheres may be good candidates for the fabrication of hydroxyapatite/collagen composite scaffolds.

In the present work, the (Zn)-doped mesoporous hydroxyapatite microspheres (Zn-MHMs) with 2 and 5 mol% of Zn substitution were synthesized through a microwave-hydrothermal method using creatine phosphate as an organic phosphorus source. The Zn-MHMs were first explored for drug delivery using doxorubicin hydrochloride (DOX) as a model drug. Furthermore, a novel biomimetic Zn-MHMs/Coll composite scaffold was constructed by incorporating the Zn-MHMs into collagen matrix through a lyophilization fabrication process. The cytocompatibility and osteoinductive potential of the Zn-MHMs/Coll scaffolds were evaluated *in vitro* by using the rat bone marrow-derived mesenchymal stem cells (rBMSCs), and the capacity to stimulate bone regeneration *in vivo* was assessed in a critical-sized femoral condyle defect rat model by micro-computed tomography (micro-CT) measurement and histological assay.

Materials and methods

Synthesis and characterization of Zn-MHMs

The Zn-MHMs with designed Zn/(Zn + Ca) molar ratios of 0, 0.02, and 0.05 were synthesized through a microwave-hydrothermal method by using creatine phosphate (Sangon Biotech, Shanghai, China) as the organic phosphorus source. The obtained products were labeled as MHMs, Zn2-MHMs, and Zn5-MHMs. In a typical synthesis of Zn5-MHMs, 0.2109 g CaCl₂ and 0.0136 g ZnCl₂ were first dissolved in 25 mL of deionized water. Then, an aqueous solution (15 mL) containing creatine phosphate (0.3926 g) was added dropwise to the above solution under constant stirring. The resulting solution was transferred into an autoclave (60 mL) and heated in a microwave oven (MDS-6; Sineo, Shanghai, China) at 100°C for 10 min. After cooling to the ambient temperature, the products were collected by centrifugation. The products of MHMs and Zn2-MHMs were synthesized under the same conditions as described earlier but by varying the Zn/(Zn + Ca) molar ratios of 0 and 0.02.

The as-obtained products were characterized by powder X-ray diffraction (XRD, Rigaku D/max 2550 V [Rigaku, Tokyo, Japan], Cu_{Kα} radiation, λ=1.54178 Å), scanning electron microscopy (SEM, FEI Magellan 400; FEI, Hillsboro, OR, USA), transmission electron microscopy (TEM, Hitachi H-800; Hitachi, Tokyo, Japan), Brunauer–Emmett–Teller (BET) specific surface area analysis (V-sorb 2800P; Gold APP, Beijing, China), and inductively coupled plasma optical emission spectrometer (ICP-OES, JY 2000-2; Horiba, Paris, France).

In vitro drug loading and release

For drug loading, MHMs or Zn5-MHMs (100 mg) were dispersed into 15 mL of DOX solution (Aladdin, 2 mg mL⁻¹) followed by ultrasonic treatment for 10 min. Then, the suspension was shaken with constant speed (120 rpm) in a sealed vessel at 37°C for 24 h. Finally, the DOX-loaded MHMs or Zn5-MHMs were collected by centrifugation and freeze-dried at -20°C. The DOX-loading capacities of MHMs and Zn5-MHMs were determined by measuring the DOX concentrations in the adsorbed supernatants using an ultraviolet–visible (UV-Vis) spectrophotometer (UV-2300; Techcomp, Shanghai, China) at 480 nm wavelength.

For the drug release assay, 20 mg of DOX-loaded MHMs or Zn5-MHMs was immersed into 15 mL of phosphate-buffered solution (PBS) at different pH values (7.4, 6.0, and 4.5) and shaken with constant speed (120 rpm) at 37°C. At given time intervals, the release medium (0.5 mL) was withdrawn for analysis with UV-Vis absorption spectroscopy at 480 nm wavelength and replaced with the same volume of fresh PBS.

rBMSCs isolation and culture

The rBMSCs were obtained from the femur and tibia of 4-week-old Sprague–Dawley (SD) rats. Briefly, the bone marrow was flushed out from the diaphysis with complete medium (CM, Dulbecco's Modified Eagle's Medium; Thermo Fisher Scientific, Waltham, MA, USA) supplemented with 10% fetal bovine serum (Thermo Fisher Scientific) and 1% (v/v) penicillin/streptomycin (Thermo Fisher Scientific). Then the cells were cultured at 37°C in a humidified atmosphere of 5% CO₂. The nonadherent cells were removed after 48 h of culture. When they reached 80%–90% confluence, cells were passaged. The rBMSCs from passage 2 to 6 were used for the following experiments.

Scaffold fabrication

Four types of scaffolds corresponding to four groups were prepared: 1) Coll scaffold, 2) MHMs/Coll scaffold, 3) Zn2-MHMs/Coll scaffold, and 4) Zn5-MHMs/Coll scaffold. In a typical experiment, a collagen slurry (40 mg g⁻¹) was prepared by mixing the collagen sponge (Kele Biological Technology Co. Ltd, Chengdu, China) with deionized water under magnetic stirring. Then, the as-prepared microspheres were added to the collagen slurry under vigorous stirring, and the weight ratio of microspheres to collagen was 3:7. For the latter process, the as-prepared slurries were added into a 24-well plate, frozen at -20°C for 24 h and freeze-dried at -20°C for 48 h. The freeze-dried scaffolds were chemically cross-linked using 20 mM N-(3-dimethylaminopropyl)-N'-ethylcarbodiimide hydrochloride (Sigma-Aldrich Co., St Louis, MO, USA) and 8 mM N-hydroxysuccinimide (Sigma-Aldrich) in 80:20 ethanol/deionized water as described previously.³⁰ Finally, the scaffolds were rinsed with deionized water and ethanol three times, followed by sterilization with 29 kGy of ⁶⁰Co radiation.

SEM observation of the scaffolds

Scaffolds were imaged both cell-free and following culturing with rBMSCs for 7 days. The rBMSCs were seeded on the scaffolds (Φ=10×2 mm, n=3) at a density of 1×10⁵ cells/scaffold and cultured for 7 days, followed by fixation in 2.5% glutaraldehyde for 2 h and dehydration through a series of ethanol baths. After freeze-drying, the scaffolds were coated with platinum and observed using SEM.

Zn ions release test

The Zn ions release test was performed as follows: 20 mg of scaffolds (n=3) were immersed in 15 mL of PBS at 37°C under constant shaking (120 rpm) in a desk-type constant-temperature oscillator (THI-92A; Peiying, Suzhou, China). At given time intervals, 3 mL of release medium was

collected to measure the concentration of Zn ions using ICP-OES and replaced with the same volume of fresh PBS.

Cell viability on scaffolds

The viability of rBMSCs on the scaffolds was evaluated using the Cell Counting Kit-8 assay (CCK-8; Dojindo Molecular Technologies Inc., Kumamoto, Japan). Briefly, the scaffolds ($\Phi=10\times 2$ mm, $n=3$) were placed into a 48-well plate and seeded with rBMSCs at a density of 1×10^5 cells/scaffold. At days 1, 3, and 7, the medium was removed, and 500 μ L of fresh medium containing 10% CCK-8 solution was added to each well. After incubation for 2 h, aliquots (100 μ L) from each well were transferred to a 96-well plate for measurement. The absorbance was measured using a microplate reader (Bio-Rad 680; Bio-Rad Laboratories Inc., Hercules, CA, USA) at 450 nm wavelength.

Cytoskeleton staining

The rBMSCs were seeded on the scaffolds ($\Phi=10\times 2$ mm, $n=3$) at a density of 1×10^5 cells/scaffold and cultured for 7 days. Then, the samples were rinsed and fixed in 4% paraformaldehyde for 30 min, followed by a pretreatment with Triton X-100 (0.5% v/v) for 5 min. Subsequently, the samples were stained with phalloidin-fluorescein isothiocyanate (FITC) (Sigma-Aldrich) and 4',6-diamidino-2-phenylindole (DAPI) (Sigma-Aldrich) successively in darkness for 30 and 5 min, respectively, and observed using a confocal laser scanning microscope (LSM 510 meta; Zeiss, Jena, Germany).

Gene expression analysis

The effects of the scaffolds on the osteogenesis-related gene expression of rBMSCs were assessed by real-time quantitative polymerase chain reaction (RT-qPCR). Briefly, the rBMSCs were seeded on the scaffolds ($\Phi=10\times 2$ mm, $n=3$) at a density of 2×10^5 cells/scaffold. At days 7 and 14, total RNA was isolated from cells on the scaffolds by homogenization in 1 mL of Trizol reagent (Thermo Fisher Scientific). Then, 500 ng of RNA was reversed transcribed into complementary DNA (cDNA) using PrimeScript 1st Strand cDNA Synthesis kit (Takara, Shiga, Japan) according to the manufacturer's instructions. Quantification of cDNA was performed on an ABI7500 Thermal Cycler (Applied Biosystems, Carlsbad, CA, USA) by using a RT-PCR kit (SYBR Premix EX Taq; Takara). All assays were run in triplicate in three independent experiments. The primers for the selected genes were as follows: *Alp* (forward: TTCATAATTCCAGGCCGAAC; reverse: GGTTCACTCATGGAGGGTGT), *Ocn* (forward: AGGACCCTCTCTGCTCACT; reverse: ACCTTAC TGCCCTCCTGCTT), *Runx2* (forward: CCACCACTCA

CTACCACACG; reverse: GGACGCTGACGAAGT ACCAT), *Gapdh* (forward: GACATGCCGCTGG AGAAAC; reverse: AGCCCAGGATGCCCTTTAGT).

Results were normalized to the level of housekeeping gene *Gapdh*. The expression of the selected genes of rBMSCs on the MHMs/Coll and Zn-MHMs/Coll scaffolds was compared with that of cells on Coll scaffolds. The relative expression was calculated using the $2^{-\Delta\Delta Ct}$ method.

Animal surgical procedures

All animal procedures were conducted in accordance with guidelines established by the Animal Research Committee of Sixth People's Hospital, Shanghai Jiao Tong University School of Medicine, and this study was approved by this committee. Eighteen male SD (200–250 g) rats were randomly allocated into the following study groups: 1) Coll scaffold ($n=6$), 2) MHMs/Coll scaffold ($n=6$), and 3) Zn5-MHMs/Coll scaffold ($n=6$). After anesthesia, a lateral linear incision of ~ 1.5 cm was made on the lateral side of knee joint, followed by blunt dissection of the muscle to expose the femoral condyle. A bone tunnel 3.5 mm in diameter and 4 mm in depth was created perpendicular to the femoral condyle using a trephine under constant irrigation with normal saline. Then, a plug bone defect was created in the femoral condyle after removing the bone fragments. Finally, the defects were implanted with the Coll, MHMs/Coll, or Zn5-MHMs/Coll scaffolds ($\Phi=3.5\times 4$ mm), and the incisions were closed layer by layer by using absorbable suture.

Micro-CT analysis

Eight weeks following operation, the rats were sacrificed. The femoral condyles were collected and fixed in 10% formaldehyde solution for 48 h. Subsequently, the specimens were scanned using micro-CT (SkyScan 1176; SkyScan, Kontich, Belgium) at a resolution of 18 μ m. The following experimental settings were used: an X-ray voltage of 65 kVp, an anode current of 278 μ A, and an exposure time of 520 ms for each of the 180 rotational steps. 3D images were reconstructed by using CTVox program (SkyScan). Bone volume to total volume ratio (BV/TV), trabecular number (Tb.N), trabecular spacing (Tb.Sp), and trabecular thickness (Tb.Th) in the defects were measured by using the CTAn program (SkyScan).

Histological observation

Following micro-CT scanning, the specimens were decalcified, dehydrated in ascending concentrations of ethanol solutions, and subsequently embedded in paraffin. Then, 5 μ m-thick coronal sections of each specimen were prepared at the central region of the defects and stained

with hematoxylin and eosin (HE), the dense and wax-like collagen distributed with nuclei was identified as the newly formed bone. Histo-morphometry analysis was performed on representative images ($n=5$) of sections from each group by using an ImageJ image analysis software (National Institutes of Health [NIH], Bethesda, MD, USA). New bone area (%) = new bone area in each section/total area.

Statistical analysis

The data were presented as mean \pm standard deviation. One-way analysis of variance and Tukey's post hoc tests were performed to determine the level of significance. Significant differences were accepted at $P < 0.05$.

Results

Characterization of the Zn-MHMs

Figure 1 shows the morphologies of the MHMs, Zn2-MHMs, and Zn5-MHMs observed by using SEM and TEM. It can be seen that all the products consisted of hydroxyapatite nanosheets that were hierarchically assembled into mesoporous hollow microspheres. These microspheres exhibited a relatively uniform size with an average diameter of $\sim 1.5 \mu\text{m}$. Inset in Figure 1H shows the energy dispersive

spectroscopy (EDS) element mapping for the distribution of Zn, Ca, P, and O within Zn5-MHMs, indicating that Zn was homogeneously distributed within the Zn5-MHMs. As shown in Table 1, the Zn/(Zn + Ca) molar ratios in the MHMs, Zn2-MHMs, and Zn5-MHMs determined by ICP-OES were 0%, 3.03%, and 7.52%, respectively, which was higher than the nominal Zn/(Zn + Ca) molar ratios.

Figure 2A shows the XRD patterns of the MHMs, Zn2-MHMs, and Zn5-MHMs. It was clear that all the products were identified as a single phase of hydroxyapatite (JCPDS 09-0432). The BET specific surface area (S_{BET}) of the MHMs, Zn2-MHMs, and Zn5-MHMs were 83.5, 105.7, and $131.0 \text{ m}^2 \text{ g}^{-1}$, respectively, and the Barrett-Joyner-Halenda (BJH) desorption cumulative pore volumes (V_p) of the MHMs, Zn2-MHMs, and Zn5-MHMs were 0.59, 0.60, and $0.70 \text{ cm}^3 \text{ g}^{-1}$, respectively (Figure 2B). The average BJH desorption pore sizes of MHMs, Zn2-MHMs, and Zn5-MHMs were 16.26, 12.81, and 8.49 nm, respectively (Figure 2C).

In vitro study of drug loading and release properties

The DOX-loading capacities of MHMs and Zn5-MHMs were 70.4 and 148.0 mg g^{-1} , respectively. As shown in Figure 3A

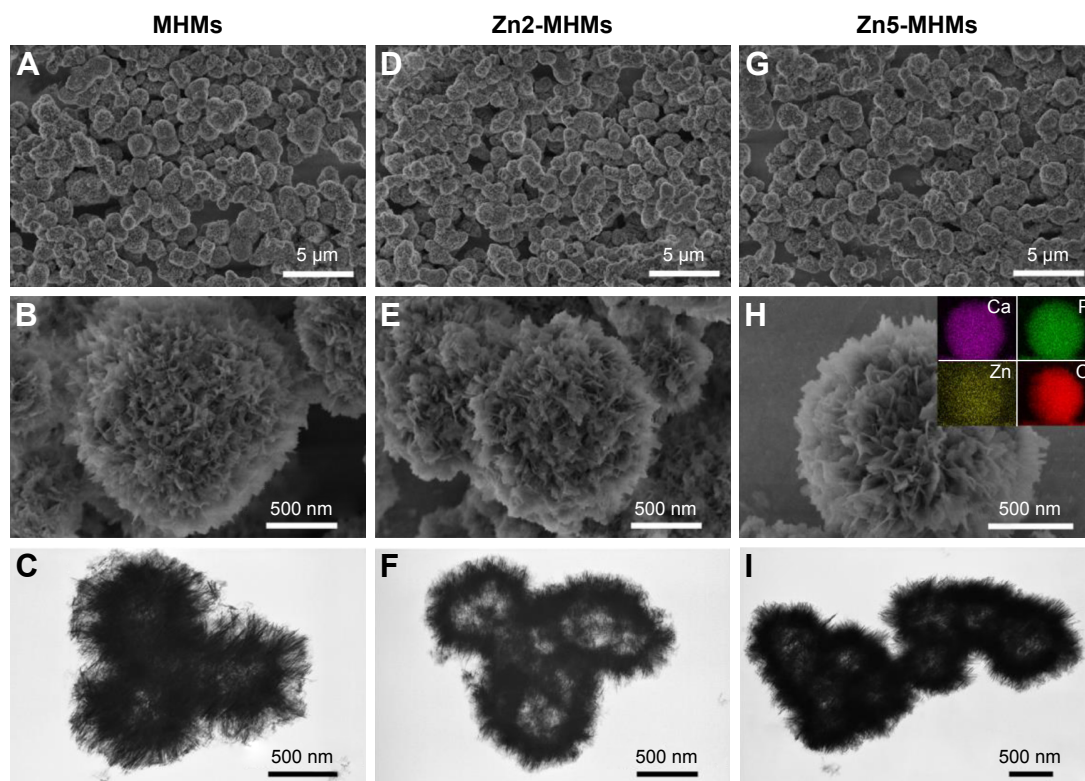


Figure 1 SEM (top and middle rows) and TEM (bottom row) images: (A–C) MHMs, (D–F) Zn2-MHMs, (G–I) Zn5-MHMs. Inset in (H) shows the EDS element mapping for the distribution of Zn, Ca, P, and O in Zn5-MHMs.

Abbreviations: SEM, scanning electron microscopy; TEM, transmission electron microscopy; MHM, mesoporous hydroxyapatite microsphere; EDS, energy dispersive spectroscopy.

Table 1 Elemental composition of different samples measured by ICP-OES

Sample name	Nominal Zn/(Zn + Ca) (%)	Measured Zn/(Zn + Ca) (%)	Nominal (Zn + Ca)/P	Measured (Zn + Ca)/P
MHMs	0	0	1.67	1.42
Zn2-MHMs	2	3.03	1.67	1.45
Zn5-MHMs	5	7.52	1.67	1.43

Abbreviations: ICP-OES, inductively coupled plasma optical emission spectrometer; MHM, mesoporous hydroxyapatite microsphere.

and B, both MHMs and Zn5-MHMs drug delivery systems exhibited a pH-responsive drug release behavior. As the pH of the medium decreased, the release rates of DOX became faster at the early stage of the drug release process. As time extends, the drug release rates of the MHMs and Zn5-MHMs drug delivery systems decreased gradually and reached a plateau. The cumulative release of DOX from the MHMs at pH values of 7.4, 6.0, and 4.5 was ~308 μg (23.45%), 781 μg (59.39%), and 1,057 μg (80.36%), respectively. And the cumulative release of DOX from the Zn5-MHMs at pH values of 7.4, 6.0, and 4.5 was ~546 μg (21.19%), 1,361 μg (52.79%), and 2,032 μg (78.81%), respectively.

Figure 3C and D shows the relationships between the cumulative amount of released DOX and the square root of the release time for the MHMs and Zn5-MHMs drug delivery systems at different pH values, both exhibiting good linear relationships with high regression factors of >0.95.

Characterization of the scaffolds

As shown in Figure 4A, all the four types of scaffolds were highly porous with an interconnected pore structure in the range of 100–300 μm . Higher magnification images show that the surfaces of the MHMs/Coll, Zn2-MHMs/Coll, and Zn5-MHMs/Coll scaffolds were rough and homogeneously

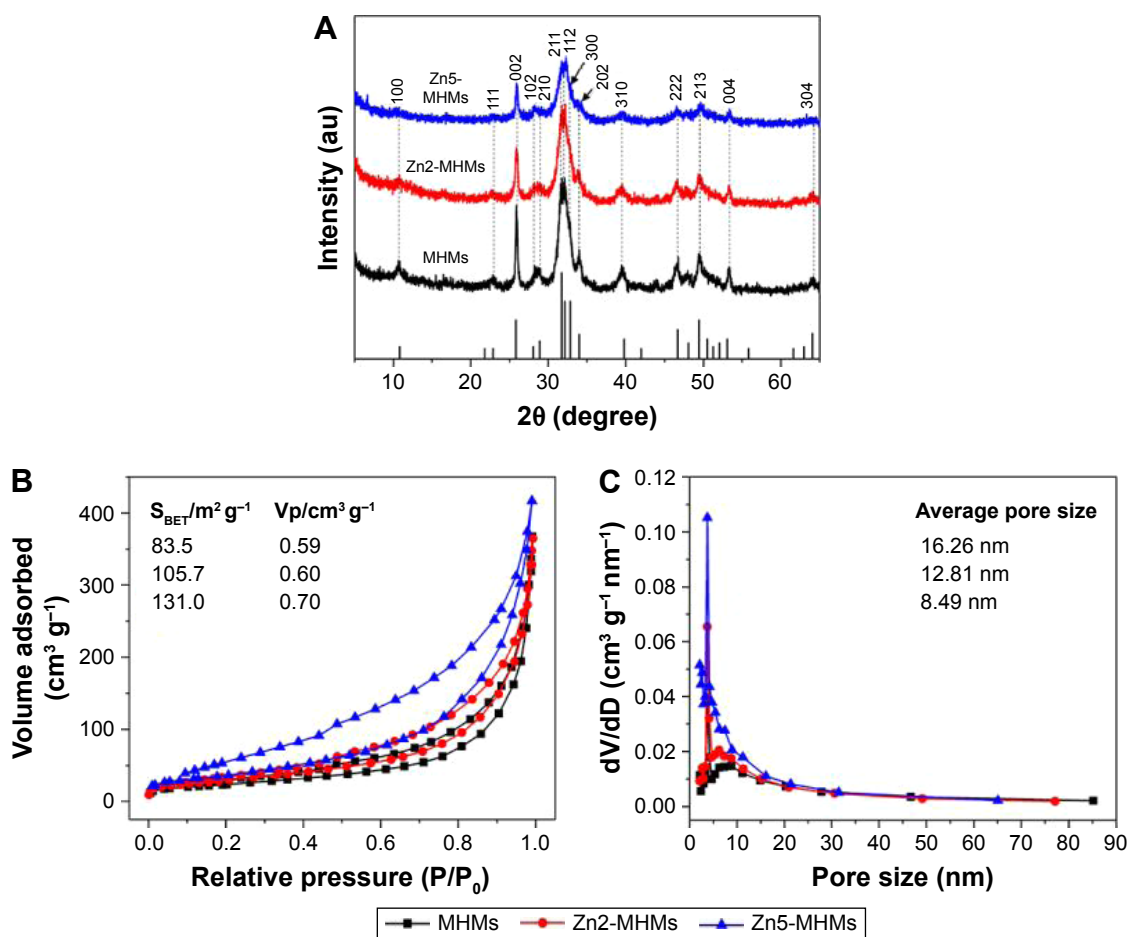


Figure 2 Physical characteristics of the MHMs, Zn2-MHMs, and Zn5-MHMs. (A) XRD patterns. (B) Nitrogen adsorption-desorption isotherms. (C) BJH pore size distributions.

Abbreviations: MHM, mesoporous hydroxyapatite microsphere; XRD, X-ray diffraction; BJH, Barrett-Joyner-Halenda; dV/dD , $d(\text{volume adsorbed})/d(\text{diameter})$.

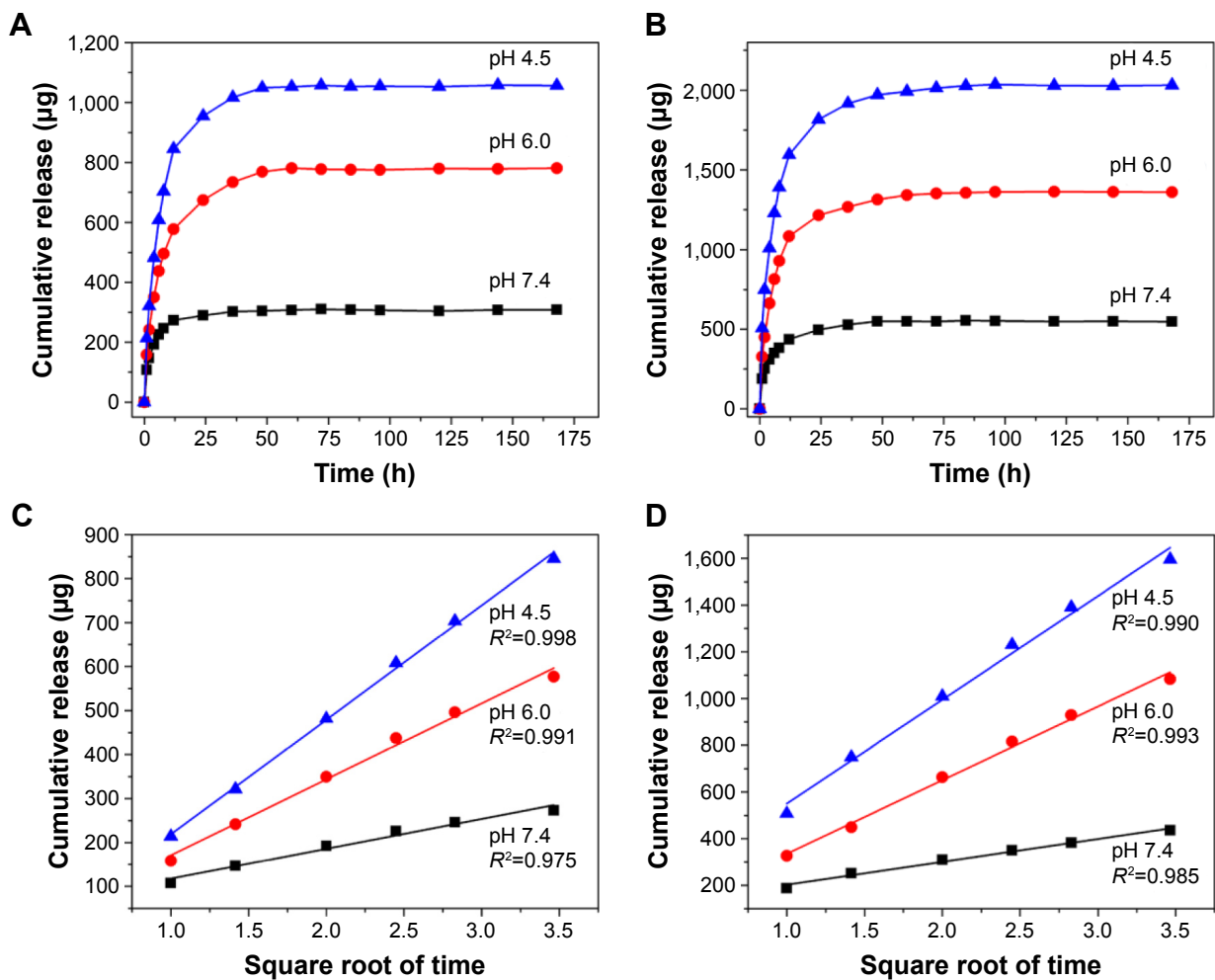


Figure 3 Drug release curves of (A) DOX-loaded MHMs and (B) DOX-loaded Zn5-MHMs in PBS solutions at different pH values. Cumulative release of DOX from (C) MHMs and (D) Zn5-MHMs as a function of the square root of the release time.

Abbreviations: DOX, doxorubicin hydrochloride; MHM, mesoporous hydroxyapatite microsphere; PBS, phosphate-buffered solution.

embedded with spherical particles, whereas the surface of the Coll scaffolds was quite smooth.

As shown in Figure 4B, both the Zn2-MHMs/Coll and Zn5-MHMs/Coll scaffolds exhibited sustained release of Zn ions in PBS. The initial rapid release of Zn ions from the Zn2-MHMs/Coll and Zn5-MHMs/Coll scaffolds in the first 4 days was 56.4 and 122.8 µg, respectively. As time extends, the release of Zn ions from the Zn2-MHMs/Coll and Zn5-MHMs/Coll scaffolds became slower and trended toward an equilibrium release stage, and the cumulative release amounts of Zn ions from the Zn2-MHMs/Coll and Zn5-MHMs/Coll scaffolds for 21 days were ~84.7 and 163.0 µg, respectively.

Cell adhesion and viability on the scaffolds

The cytoskeleton staining showed that the rBMSCs attached and spread well on all the four types of collagen-based scaffolds (Figure 5A). The SEM images further showed that the

rBMSCs presented a well-spreading morphology with clear and prominent filopodia on the scaffolds (Figure 5B).

As determined by CCK-8 assay (Figure 5C), there was no apparent drop in cell number for all the four types of scaffolds across the culture period. However, compared to the Coll scaffolds, the MHMs/Coll, Zn2-MHMs/Coll, and Zn5-MHMs/Coll scaffolds showed lower cell viability at days 3 and 7.

Osteogenic induction in vitro

The rBMSCs were cultured directly on the scaffolds to assess the expression of osteogenesis-related genes (Figure 6). Compared to those cultured on the Coll scaffolds, the rBMSCs cultured on the MHMs/Coll, Zn2-MHMs/Coll and Zn5-MHMs/Coll composite scaffolds showed increased expression levels of *Runx2*, *Alp*, and *Ocn* at days 7 and 14. Moreover, the expression levels of these genes increased with increasing Zn content in the Zn-MHMs/Coll scaffolds. However, the expression of *Runx2* was not significantly

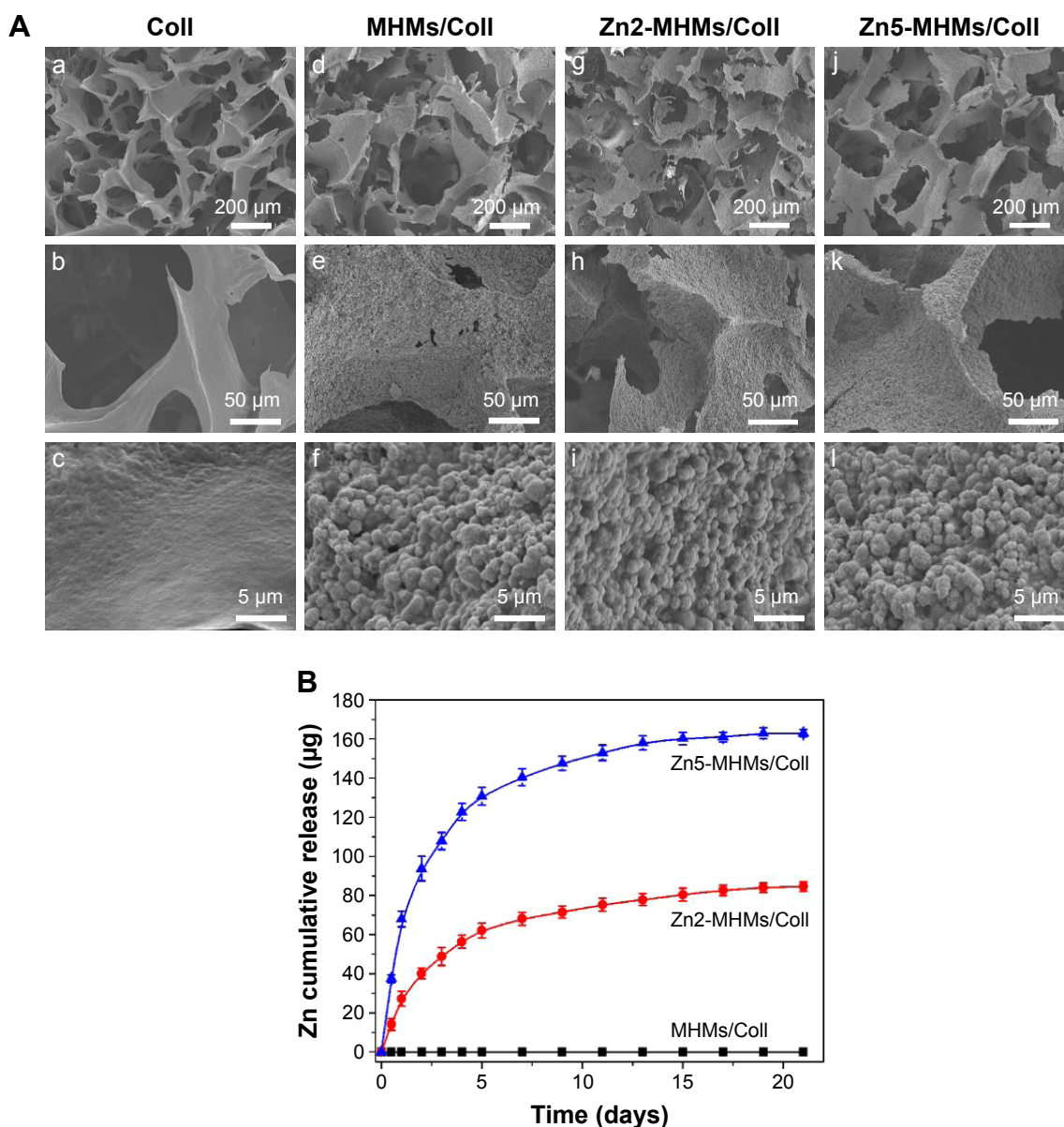


Figure 4 Physical characteristics of the Coll, MHMs/Coll, Zn2-MHMs/Coll, and Zn5-MHMs/Coll scaffolds. **(A)** SEM micrographs of the Coll (a–c), MHMs/Coll (d–f), Zn2-MHMs/Coll (g–i), and Zn5-MHMs/Coll scaffolds (j–l). **(B)** Release of Zn ions from the MHMs/Coll, Zn2-MHMs/Coll, and Zn5-MHMs/Coll scaffolds.

Abbreviations: MHMs/Coll, mesoporous hydroxyapatite microspheres/collagen scaffold; SEM, scanning electron microscopy.

elevated ($P>0.05$) for the cells cultured on the MHMs/Coll and Zn2-MHMs/Coll scaffolds at day 14, and the expression of *Ocn* was not significantly elevated ($P>0.05$) for the cells cultured on the MHMs/Coll and Zn2-MHMs/Coll scaffolds at day 7 compared with those cultured on the Coll scaffolds.

Micro-CT measurement

To evaluate new bone formation in the rat femoral condyle bone defects, micro-CT was performed after 8 weeks of implantation. As shown in Figure 7A, no new bone was formed in the central area of the defects implanted with the Coll scaffolds, and more new bones were formed in the

Zn5-MHMs/Coll group compared with the MHMs/Coll group. Furthermore, the morphometric analysis showed that the BV/TV in Zn5-MHMs/Coll group ($56.76\pm4.46\%$) was significantly higher ($P<0.05$) than that in the MHMs/Coll group ($40.18\pm4.41\%$) or Coll group ($22.87\pm4.46\%$) (Figure 7B), and the Tb.N in Zn5-MHMs/Coll group ($2.18\pm0.33/\text{mm}$) was significantly greater ($P<0.05$) than that in the MHMs/Coll group ($1.65\pm0.07/\text{mm}$) or Coll group ($1.10\pm0.12/\text{mm}$) (Figure 7C). The Tb.Sp in Zn5-MHMs/Coll group (0.31 ± 0.05 mm) and MHMs/Coll group (0.56 ± 0.10 mm) was significantly lower ($P<0.05$) than that in the Coll group (1.63 ± 0.37 mm) (Figure 7D), and

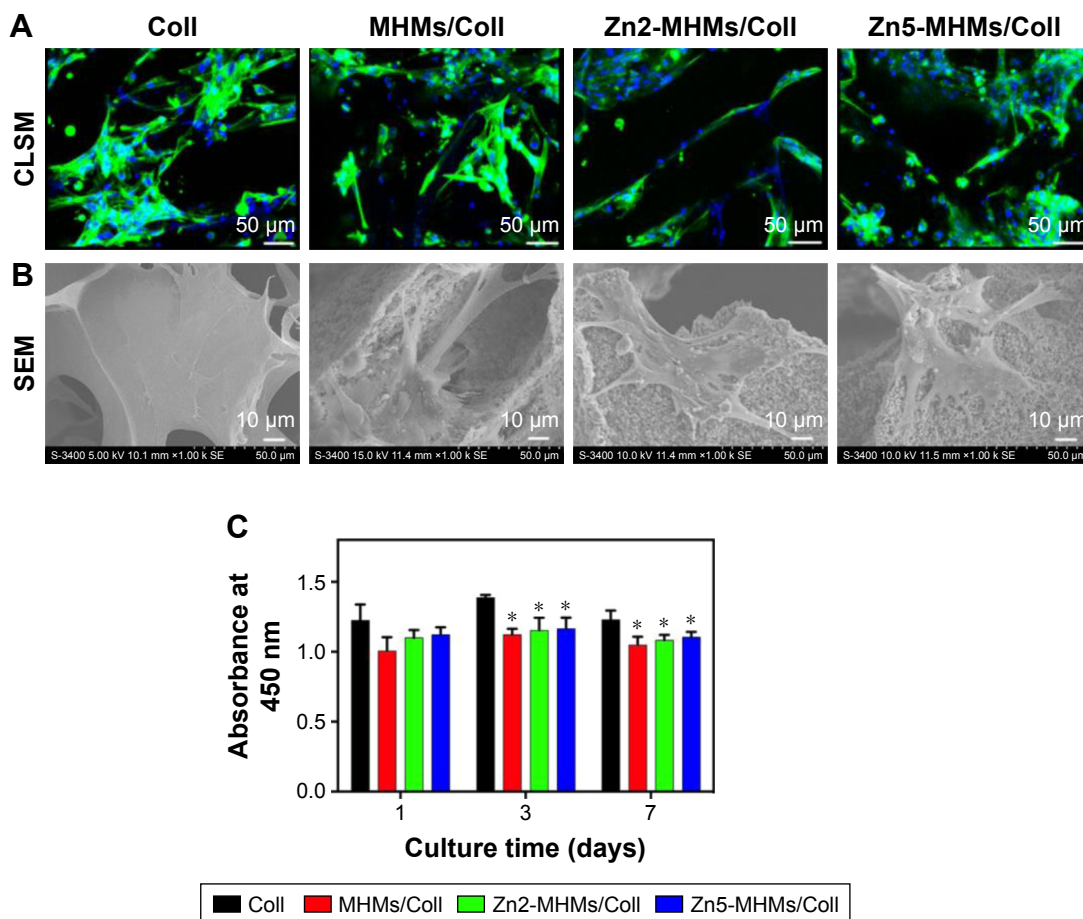


Figure 5 Cell morphology observation and viability assay on the Coll, MHMs/Coll, Zn2-MHMs/Coll, and Zn5-MHMs/Coll scaffolds. (A and B) CLSM and SEM images of rBMSCs on each type of scaffold after 7 days of culture. (C) Quantitative evaluation of the viability of rBMSCs on the four types of scaffolds at days 1, 3, and 7. * $P < 0.05$ compared to Coll scaffolds.

Abbreviations: MHMs/Coll, mesoporous hydroxyapatite microspheres/collagen scaffold; CLSM, confocal laser scanning microscope; SEM, scanning electron microscopy; rBMSC, rat bone marrow-derived mesenchymal stem cell.

no significant difference ($P > 0.05$) was observed in Tb.Th among the three groups (Figure 7E).

Histological assessment of bone regeneration in the femoral condyle defects

HE staining of representative sections from each group is shown in Figure 8A. In the Coll group, the defect area was mainly occupied by connective tissue, and the newly formed bone structure was observed only near the border of the defects. In the MHMs/Coll group, more bone tissues were observed within the defects compared with the Coll group. Encouragingly, markedly greater amounts of new bone occupied the whole defects implanted with the Zn5-MHMs/Coll scaffolds. Histomorphometric analysis showed trends for new bone formation which were in agreement with the micro-CT data (Figure 8B). The percentage of new bone area in the Zn5-MHMs/Coll group ($42.27\% \pm 5.74\%$) was significantly

greater ($P < 0.05$) than that in the MHMs/Coll group ($32.55\% \pm 5.66\%$) or Coll group ($13.16\% \pm 3.92\%$). Scaffold remnants were still present in the defect site at 8 weeks post implantation. All scaffolds from each group were observed to integrate well with the peripheral host tissue.

Discussion

In the present study, the Zn-MHMs were successfully synthesized by using creatine phosphate as the organic phosphorus source through a microwave-hydrothermal method. The Zn-MHMs with a mesoporous hollow structure and a high specific surface area were efficient in drug delivery and showed a pH-responsive drug release behavior by using DOX as a model drug. Furthermore, a biomimetic bone tissue engineering scaffold was constructed by incorporating the Zn-MHMs into collagen matrix with a view to mimicking the structure and composition of human trabecular bone and more importantly enhancing the bone formation ability.

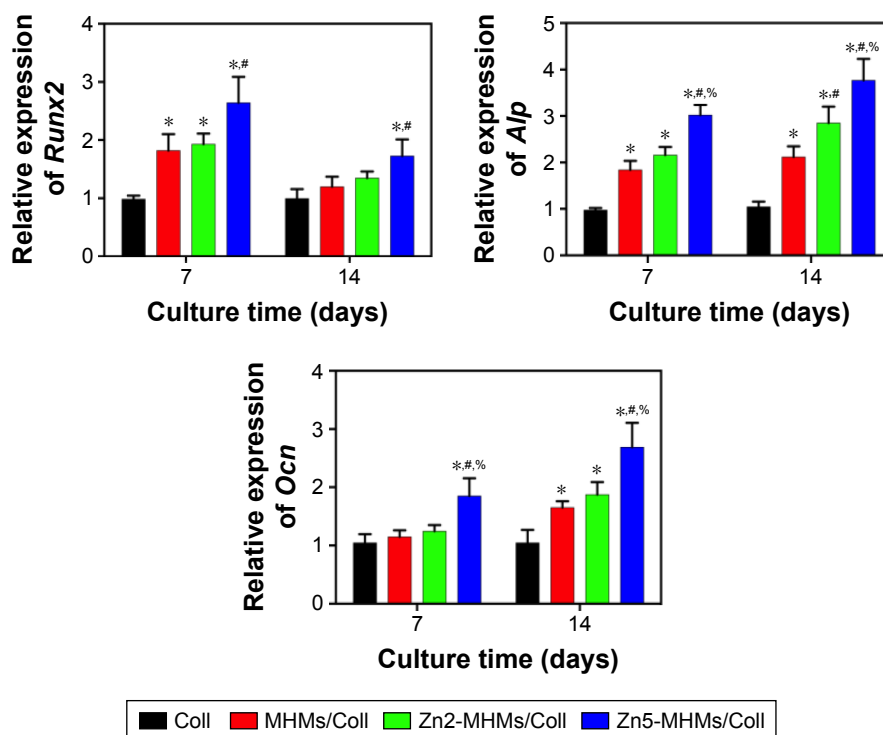


Figure 6 RT-qPCR analysis of the expression of osteogenesis-related genes (*Runx2*, *Alp*, and *Ocn*) in rBMSCs cultured on the Coll, MHMs/Coll, Zn2-MHMs/Coll, and Zn5-MHMs/Coll scaffolds for 7 and 14 days. * $P < 0.05$ compared to Coll scaffolds; # $P < 0.05$ compared to MHMs/Coll scaffolds; % $P < 0.05$ compared to Zn2-MHMs/Coll scaffolds. **Abbreviations:** RT-qPCR, real-time quantitative polymerase chain reaction; MHMs/Coll, mesoporous hydroxyapatite microspheres/collagen scaffold; rBMSC, rat bone marrow-derived mesenchymal stem cell.

The Zn-MHMs were synthesized through a microwave-hydrothermal process, which has been demonstrated to be an efficient, rapid, energy-saving method for the fabrication of CaP nanostructured porous microspheres.^{28,29} Compared to the inorganic phosphorus sources such as Na_2HPO_4 , the organic phosphorus sources play a key role in the formation of the spherical structure of hydroxyapatite.^{27,31} In this work, creatine phosphate, a biomolecule that provides energy to cells by synthesizing adenosine 5'-triphosphate, was used as the organic phosphorus source as it has been proved to be a suitable organic phosphorus source for the synthesis of hydroxyapatite microspheres.²⁷ The EDS element mapping showed that Zn was uniformly distributed within the Zn5-MHMs, indicating that Zn was successfully introduced into the MHMs. According to our previous studies,^{27,32} the mechanism for the formation of the Zn-MHMs might be as follows. Creatine phosphate molecules hydrolyze to produce creatine molecules and PO_4^{3-} ions, followed by the nuclei formation from a reaction among PO_4^{3-} , Ca^{2+} , and Zn^{2+} ions in an aqueous solution. Then, the Zn-doped hydroxyapatite nanosheets are formed through a crystal growth process under microwave-hydrothermal conditions. Finally, the Zn-doped hydroxyapatite nanosheets self-assemble to form hierarchically nanostructured Zn-MHMs driven by the minimization

of the free energy of the nanocrystals. The Zn-MHMs consisting of hydroxyapatite nanosheets showed a mesoporous hollow structure and a relatively large specific surface area, which make them favorable for drug delivery. This study investigated the drug loading and release performance of the Zn5-MHMs as the drug nanocarrier. The Zn5-MHMs drug delivery system exhibited a pH-responsive drug release behavior. The amount of DOX released from the Zn5-MHMs at pH 4.5 was much higher than that at pH 6.0 and 7.4, and the drug release rate increased in the following order: pH 7.4 < pH 6.0 < pH 4.5. The lower drug release rate at pH 7.4 may result from the strong electrostatic attraction between the negatively charged Zn5-MHMs and the positively charged DOX, which prevents the escape of DOX molecules from the Zn5-MHMs.³³ The pH-responsive drug release behavior may be derived from the pH-dependent dissolution of Zn5-MHMs drug delivery system.³⁴ Moreover, the relationships between the cumulative amount of released DOX and the square root of the release time for the Zn5-MHMs drug delivery system showed good linear relationships with high regression factors of >0.95 , indicating that the DOX release from the Zn5-MHMs is governed by Fickian diffusion of the Higuchi model.³⁵ The excellent performance in drug delivery makes Zn-MHMs a promising nanocarrier for the delivery

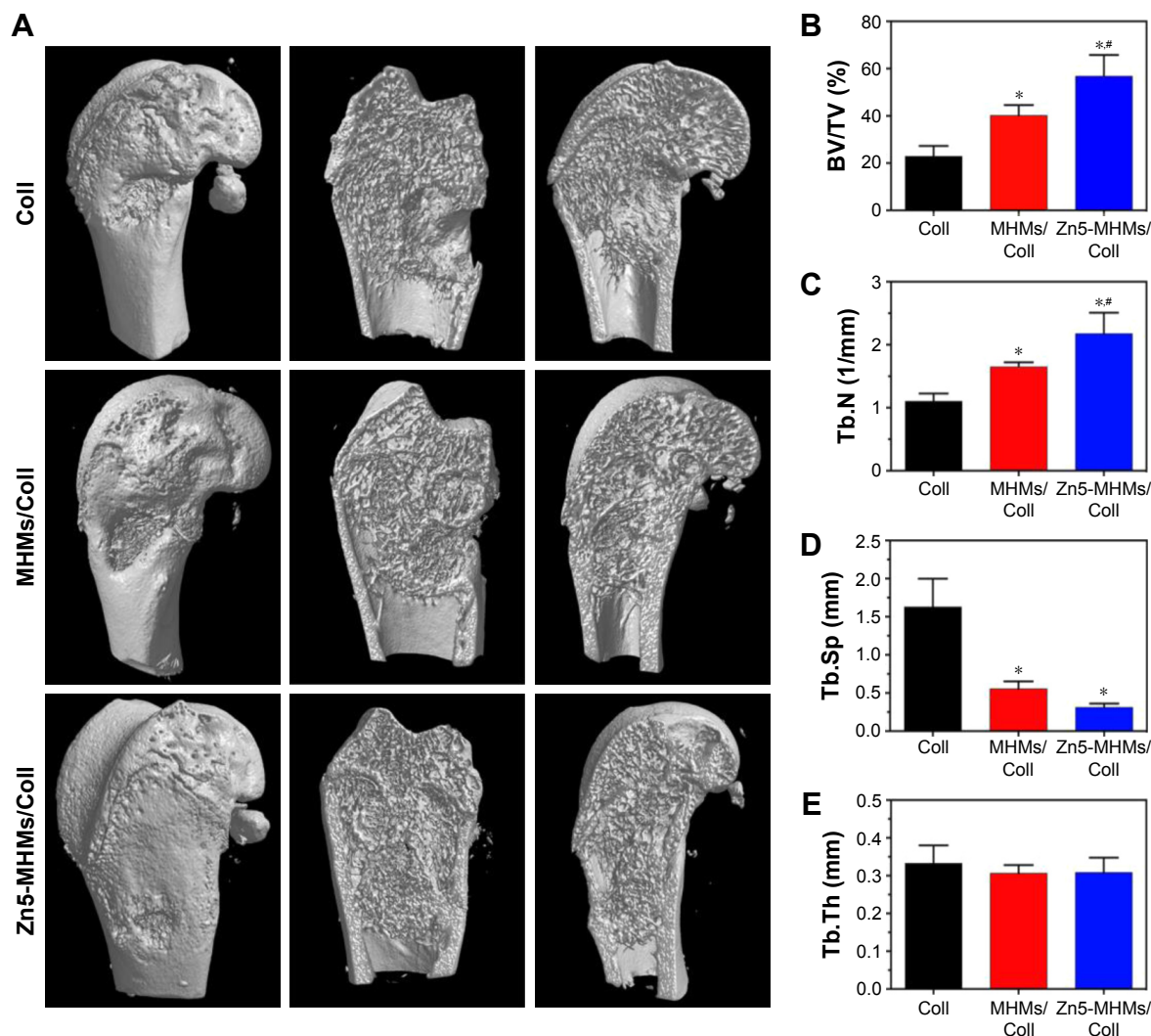


Figure 7 Micro-CT analysis of bone regeneration for the Coll, MHMs/Coll, and Zn5-MHMs/Coll groups at 8 weeks postimplantation. (A) 3D reconstructed superficial and interior images of femoral condyle defects implanted with different scaffolds. Morphometric analysis of the BV/TV (B), Tb.N (C), Tb.Sp (D), and Tb.Th (E) for each group. * $P < 0.05$ compared to Coll group; ** $P < 0.05$ compared to MHMs/Coll group.

Abbreviations: micro-CT, micro-computed tomography; MHMs/Coll, mesoporous hydroxyapatite microspheres/collagen scaffold; 3D, three dimensional; BV/TV, bone volume to total volume ratio; Tb.N, trabecular number; Tb.Sp, trabecular spacing; Tb.Th, trabecular thickness.

of osteogenic factors such as bone morphogenetic protein 2 (BMP-2). The collagen–hydroxyapatite scaffolds releasing BMP-2 in a controlled fashion has been demonstrated to increase the healing of bone defects.⁸

In this work, a biomimetic Zn-MHMs/Coll composite scaffold was fabricated by using a lyophilization fabrication process. Our working hypothesis was that scaffolds mimicking the structure and composition of the bone would stimulate osteogenesis in vitro and enhance new bone formation in vivo. The ratio of the Zn-MHMs to collagen was 7:3, which closely resembles the ratio between inorganic and organic components in osseous matrix of young human.³⁶ The Zn-MHMs/Coll composite scaffolds showed an interconnected pore network, and the pore size was in the range of

100–300 μm , which is favorable for the infiltration of cells and blood vessels.³⁷ The Zn-MHMs/Coll scaffolds showed a sustained release of Zn ions, and the release of Zn ions showed a marked dependence on the Zn content in the composite scaffolds, indicating that the release of Zn ions from the Zn-MHMs/Coll scaffolds can be controlled by modifying the content of Zn in the Zn-MHMs. However, high concentration of Zn ions may cause cell toxicity,²³ the controlled release of Zn ions from the Zn-MHMs/Coll scaffolds is therefore desirable at concentrations pertinent to stimulate osteogenic response. The concentration of Zn ions released from the Zn-MHMs/Coll scaffolds was within the range of 14.5–76.0 μM , which has been demonstrated to stimulate bone formation in tissue culture and is well below cytotoxic levels.^{20,38}

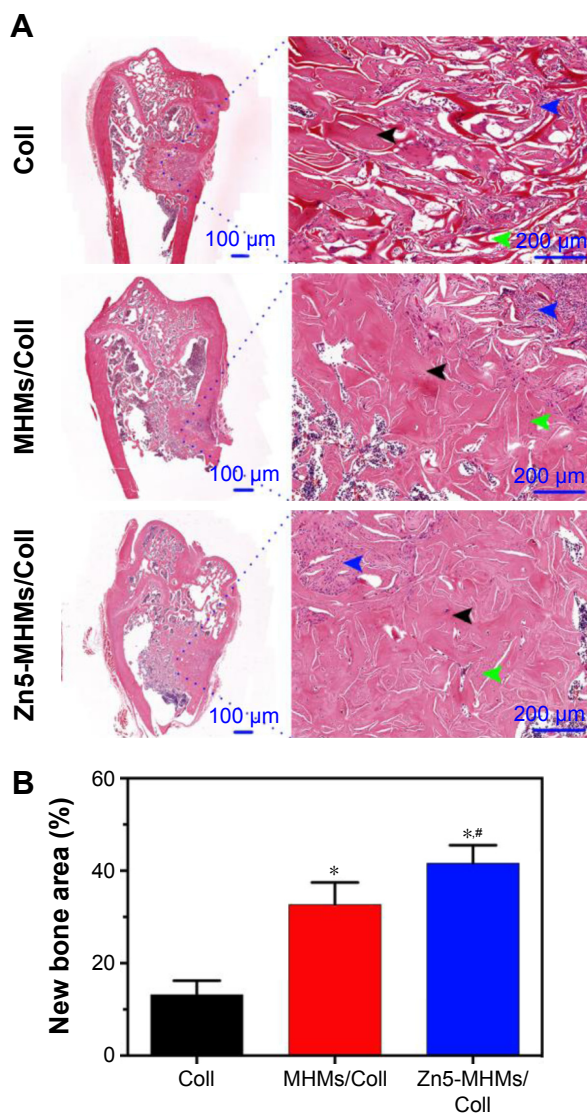


Figure 8 Histological evaluation of bone regeneration in each group. **(A)** HE staining for newly formed bone (black arrowhead), connective tissue (blue arrowhead), and scaffold remnants (green arrowhead). **(B)** The percentage of the new bone area assessed by histomorphometric analysis. * $P < 0.05$ compared to Coll group; # $P < 0.05$ compared to MHMs/Coll group.

Abbreviations: MHMs/Coll, mesoporous hydroxyapatite microspheres/collagen scaffold; HE, hematoxylin and eosin.

The rBMSCs are attached and spread well on the composite scaffolds, which are demonstrated to be biocompatible. According to the CCK-8 assay, there was no apparent reduction in cell viability during the culture period. However, on MHMs/Coll and Zn-MHMs/Coll scaffolds, cell viability was found to be lower than that on the Coll scaffolds at days 3 and 7. It was reported that the magnesium-doped hydroxyapatite/collagen scaffold mimicking the hypoxic condition in the osteogenic niche might be responsible for maintaining the cells in a quiescent state.^{9,39} On the other hand, ion-induced cell death such as that from excessive Ca^{2+} may account for lower cell viability resulting from the initial ion release from

the composite scaffolds.^{40,41} Collagen-based materials that serve as analogs of organic components of bone matrix have previously been developed for bone regeneration.^{10,42} It was hypothesized that the incorporation of MHMs or Zn-MHMs would improve the osteoinductive potential of the Coll scaffolds. Previous studies have demonstrated that hydroxyapatite could stimulate the osteogenesis of osteoblasts in vitro and induce in vivo bone formation.^{43,44} It was reported that the presence of hydrophilic hydroxyl groups ($-\text{OH}$) on a substrate, as found in hydroxyapatite, could modulate osteoblastic differentiation by enhancing the recruitment of signaling and structural biomolecules involved in cell adhesion.⁴⁵ Habibovic et al reported that the increased specific surface area of CaP ceramics led to more specific surface reactivity and further improved the osteogenic activity of the materials.⁴⁶ Reports have stated that hydroxyapatite bioceramics with nanostructured surfaces could promote protein adsorption, osteoblast proliferation, osteogenic differentiation, and in vivo bone formation.^{47,48} Moreover, naive mesenchymal stem cells are demonstrated to be extremely sensitive to the tissue elasticity, and rigid matrices that mimic collagenous bone have been proven to be osteogenic.⁴⁹ The incorporation of MHMs or Zn-MHMs might improve the mechanical properties of the Coll scaffolds as a result of the reinforcing effect of the microspheres. Cunniffe et al reported that the nanosized hydroxyapatite particles could improve the mechanical properties of collagen-based scaffolds resulting from their high specific surface area and strong bonding.¹¹ With all this in mind, the osteoinductive potential of the MHMs/Coll and Zn-MHMs/Coll scaffolds was explored by examining their capacities to induce osteogenesis of the rBMSCs and new bone formation in a rat femoral condyle defect model. As expected, the MHMs/Coll and Zn-MHMs/Coll scaffolds enhanced the osteogenic differentiation of rBMSCs and in vivo new bone formation compared with the Coll scaffolds. The Zn5-MHMs/Coll scaffolds showed higher osteogenic activity in vitro and achieved a superior repair of bone defects compared with the MHMs/Coll scaffolds, indicating that the introduction of Zn improves the osteoinductivity of the scaffolds. The Zn5-MHMs/Coll scaffolds may potentially provide a better microenvironment resembling the osteoblastic niche for bone augmentation compared with the Coll or MHMs/Coll scaffolds in terms of inducing osteogenesis of mesenchymal stem cells. Luo et al reported that Zn-containing tricalcium phosphate induced a great amount of new bone formation in the paraspinal muscle of canines.²⁶ The mechanism by which Zn influenced the osteogenic differentiation of the rBMSCs was beyond the scope of the present work. However, recent

studies reported that Zn transporter-mediated Zn ions behaving as a signaling factor called Zn signal may play a crucial role in cellular events involving bone homeostasis.⁵⁰ Overall, the introduction of Zn endows the Zn-MHMs and Zn-MHMs/Coll scaffolds with enhanced osteoinductive potential beneficial for bone augmentation.

Conclusion

In this study, novel Zn-MHMs were synthesized through a microwave-hydrothermal method by producing phosphate as an organic phosphorus source. Zn-MHMs consisting of hydroxyapatite nanosheets as the building blocks showed a hierarchically mesoporous hollow structure and a high specific surface area, which are beneficial for drug delivery and tissue engineering. A novel biomimetic Zn-MHMs/Coll composite scaffold was constructed by incorporating Zn-MHMs into collagen matrix with a view to mimicking the structure and composition of human trabecular bone and improving the osteoinductive potential. Compared with the Coll and MHMs/Coll scaffolds, the Zn-MHMs/Coll scaffolds enhanced the osteogenic differentiation of the rBMSCs and encouraged more rapid and superior bone formation and healing, which bodes well for their future applications in bone defect repair and regeneration.

Acknowledgments

Financial support from the National High-Tech Research and Development Program of China (863-Project, No 2015AA020316), National Natural Science Foundation of China (81271961, 81572106, 81271998, 81601886), and the Science and Technology Commission of Shanghai, China (15ZR1431900, 15JC1491001) is gratefully acknowledged. The authors thank Dr Feng Chen for technical assistance.

Disclosure

The authors report no conflicts of interest in this work.

References

- Vallet-Regi M, Ruiz-Hernandez E. Bioceramics: from bone regeneration to cancer nanomedicine. *Adv Mater*. 2011;23(44):5177–5218.
- Habibovic P, Barralet JE. Bioinorganics and biomaterials: bone repair. *Acta Biomater*. 2011;7(8):3013–3026.
- Dimitriou R, Jones E, McGonagle D, Giannoudis PV. Bone regeneration: current concepts and future directions. *BMC Med*. 2011;9(1):1–10.
- Bucholz RW. Nonallograft osteoconductive bone graft substitutes. *Clin Orthop Relat Res*. 2002;(395):44–52.
- Arrington ED, Smith WJ, Chambers HG, Bucknell AL, Davino NA. Complications of iliac crest bone graft harvesting. *Clin Orthop Relat Res*. 1996;(329):300–309.
- Marino A, Filipeschi C, Genchi GG, Mattoli V, Mazzolai B, Ciofani G. The Osteoprint: a bioinspired two-photon polymerized 3-D structure for the enhancement of bone-like cell differentiation. *Acta Biomater*. 2014;10(10):4303–4313.
- Marino A, Barsotti J, De VG, et al. Two-photon lithography of 3D nanocomposite piezoelectric scaffolds for cell stimulation. *ACS Appl Mater Interfaces*. 2015;7(46):25574–25579.
- Quinlan E, Thompson EM, Matsiko A, O'Brien FJ, Lopez-Noriega A. Long-term controlled delivery of rhBMP-2 from collagen-hydroxyapatite scaffolds for superior bone tissue regeneration. *J Controlled Release*. 2015;207:112–119.
- Minardi S, Corradetti B, Taraballi F, et al. Evaluation of the osteoinductive potential of a bio-inspired scaffold mimicking the osteogenic niche for bone augmentation. *Biomaterials*. 2015;62:128–137.
- Kane RJ, Weiss-Bilka HE, Meagher MJ, et al. Hydroxyapatite reinforced collagen scaffolds with improved architecture and mechanical properties. *Acta Biomater*. 2015;17(6):16–25.
- Cunniffe GM, Curtin CM, Thompson EM, Dickson GR, O'Brien FJ. Content-dependent osteogenic response of nanohydroxyapatite: an in vitro and in vivo assessment within collagen-based scaffolds. *ACS Appl Mater Interfaces*. 2016;8(36):23477–23488.
- Raisz LG. Physiology and pathophysiology of bone remodeling. *Clin Chem*. 1999;45(8 Pt 2):1353–1358.
- Katz EP, Li ST. Structure and function of bone collagen fibrils. *J Mol Biol*. 1973;80(1):1–15.
- Yang M, Zhou G, Castano-Izquierdo H, Zhu Y, Mao C. Biomimetic mineralization of natural collagenous nanofibrous membranes and their potential use in bone tissue engineering. *J Biomed Nanotechnol*. 2015;11(3):447–456.
- Landi E, Celotti G, Logroscino G, Tampieri A. Carbonated hydroxyapatite as bone substitute. *J Eur Ceram Soc*. 2003;23(15):2931–2937.
- Beattie JH, Avenell A. Trace element nutrition and bone metabolism. *Nutr Res Rev*. 1992;5(1):167–188.
- Zofková I, Nemicikova P, Matucha P. Trace elements and bone health. *Clin Chem Lab Med*. 2013;51(8):1555–1561.
- Relea P, Revilla M, Ripoll E, Arribas I, Villa LF, Rico H. Zinc, biochemical markers of nutrition, and type I osteoporosis. *Age Ageing*. 1995;24(4):303–307.
- Eberle J, Schmidmayer S, Erben RG, Stangassinger M, Roth HP. Skeletal effects of zinc deficiency in growing rats. *J Trace Elem Med Biol*. 1999;13(1–2):21–26.
- Yamaguchi M, Oishi H, Suketa Y. Stimulatory effect of zinc on bone formation in tissue culture. *Biochem Pharmacol*. 1987;36(22):4007–4012.
- Seo HJ, Cho YE, Kim T, Shin HI, Kwun IS. Zinc may increase bone formation through stimulating cell proliferation, alkaline phosphatase activity and collagen synthesis in osteoblastic MC3T3-E1 cells. *Nutr Res Pract*. 2010;4(5):356–361.
- Yusa K, Yamamoto O, Fukuda M, Koyota S, Koizumi Y, Sugiyama T. In vitro prominent bone regeneration by release zinc ion from Zn-modified implant. *Biochem Biophys Res Commun*. 2011;412(412):273–278.
- Wang H, Zhao S, Xiao W, et al. Three-dimensional zinc incorporated borosilicate bioactive glass scaffolds for rodent critical-sized calvarial defects repair and regeneration. *Colloid Surf B*. 2015;130:149–156.
- Jin G, Cao H, Qiao Y, Meng F, Zhu H, Liu X. Osteogenic activity and antibacterial effect of zinc ion implanted titanium. *Colloid Surf B*. 2014;117:158–165.
- Qiao Y, Zhang W, Tian P, et al. Stimulation of bone growth following zinc incorporation into biomaterials. *Biomaterials*. 2014;35(25):6882–6897.
- Luo X, Barbieri D, Davison N, Yan Y, de Bruijn JD, Yuan H. Zinc in calcium phosphate mediates bone induction: in vitro and in vivo model. *Acta Biomater*. 2014;10(1):477–485.
- Qi C, Zhu YJ, Lu BQ, et al. Hydroxyapatite hierarchically nanostructured porous hollow microspheres: rapid, sustainable microwave-hydrothermal synthesis by using creatine phosphate as an organic phosphorus source and application in drug delivery and protein adsorption. *Chem Eur J*. 2013;19(17):5332–5341.
- Qi C, Zhu YJ, Chen F. Fructose 1,6-bisphosphate trisodium salt as a new phosphorus source for the rapid microwave synthesis of porous calcium-phosphate microspheres and their application in drug delivery. *Chem Asian J*. 2013;8(1):88–94.

29. Qi C, Zhu YJ, Zhao XY, et al. Highly stable amorphous calcium phosphate porous nanospheres: microwave-assisted rapid synthesis using ATP as phosphorus source and stabilizer, and their application in anticancer drug delivery. *Chem Eur J*. 2013;19(3):981–987.
30. Olde Damink LH, Dijkstra PJ, van Luyn MJ, van Wachem PB, Nieuwenhuis P, Feijen J. Cross-linking of dermal sheep collagen using a water-soluble carbodiimide. *Biomaterials*. 1996;17(8):765–773.
31. Qi C, Chen F, Wu J, Zhu Y-J, Hao C-N, Duan J-L. Magnesium whitlockite hollow microspheres: a comparison of microwave-hydrothermal and conventional hydrothermal syntheses using fructose 1,6-bisphosphate, and application in protein adsorption. *RSC Adv*. 2016; 6(40):33393–33402.
32. Qi C, Zhu YJ, Wu CT, et al. Sonochemical synthesis of hydroxyapatite nanoflowers using creatine phosphate disodium salt as an organic phosphorus source and their application in protein adsorption. *RSC Adv*. 2016;6(12):9686–9692.
33. Zhu YJ, Chen F. Microwave-assisted preparation of inorganic nanostructures in liquid phase. *Chem Rev*. 2014;114(12):6462–6555.
34. Qi C, Zhu YJ, Zhang YG, Jiang YY, Wu J, Chen F. Vesicle-like nanospheres of amorphous calcium phosphate: sonochemical synthesis using the adenosine 5'-triphosphate disodium salt and their application in pH-responsive drug delivery. *J Mater Chem B*. 2015;3(37):7347–7354.
35. Andersson J, Rosenholm J, Sami Areva A, Lindén M. Influences of material characteristics on ibuprofen drug loading and release profiles from ordered micro- and mesoporous silica matrices. *Chem Mater*. 2004; 16(21):4160–4167.
36. Robinson RA. Bone tissue: composition and function. *Johns Hopkins Med J*. 1979;145(1):10–24.
37. Yang S, Leong KF, Du Z, Chua CK. The design of scaffolds for use in tissue engineering. Part I. Traditional factors. *Tissue Eng*. 2001;7(6): 679–689.
38. Brauer DS, Gentleman E, Farrar DF, Stevens MM, Hill RG. Benefits and drawbacks of zinc in glass ionomer bone cements. *Biomed Mater*. 2011;6(4):1985–1992.
39. Corradetti B, Taraballi F, Powell S, et al. Osteoprogenitor cells from bone marrow and cortical bone: understanding how the environment affects their fate. *Stem Cells Dev*. 2015;24(9):1112–1123.
40. Quinlan E, Partap S, Azevedo MM, Jell G, Stevens MM, O'Brien FJ. Hypoxia-mimicking bioactive glass/collagen glycosaminoglycan composite scaffolds to enhance angiogenesis and bone repair. *Biomaterials*. 2015;52(1):358–366.
41. Alcaide M, Portolés P, López-Noriega A, Arcos D, Vallet-Regí M, Portolés MT. Interaction of an ordered mesoporous bioactive glass with osteoblasts, fibroblasts and lymphocytes, demonstrating its biocompatibility as a potential bone graft material. *Acta Biomater*. 2010; 6(3):892–899.
42. Lyons FG, Al-Munajjed AA, Kieran SM, et al. The healing of bony defects by cell-free collagen-based scaffolds compared to stem cell-seeded tissue engineered constructs. *Biomaterials*. 2010;31(35): 9232–9243.
43. Cheng L, Feng Y, Yang R, et al. Osteoinduction of hydroxyapatite/ β -tricalcium phosphate bioceramics in mice with a fractured fibula. *Acta Biomater*. 2010;6(4):1569–1574.
44. Lin L, Chow KL, Leng Y. Study of hydroxyapatite osteoinductivity with an osteogenic differentiation of mesenchymal stem cells. *J Biomed Mater Res A*. 2009;89(2):326–335.
45. Keselowsky BG, Collard DM, García AJ. Surface chemistry modulates focal adhesion composition and signaling through changes in integrin binding. *Biomaterials*. 2004;25(28):5947–5954.
46. Habibovic P, Sees TM, Doel MAVD, Blitterswijk CAV, Groot KD. Osteoinduction by biomaterials – physicochemical and structural influences. *J Biomed Mater Res A*. 2006;77(4):747–762.
47. Lin K, Xia L, Li H, et al. Enhanced osteoporotic bone regeneration by strontium-substituted calcium silicate bioactive ceramics. *Biomaterials*. 2013;34(38):10028–10042.
48. Lin K, Xia L, Gan J, et al. Tailoring the nanostructured surfaces of hydroxyapatite bioceramics to promote protein adsorption, osteoblast growth, and osteogenic differentiation. *ACS Appl Mater Interfaces*. 2013; 5(16):8008–8017.
49. Engler AJ, Sen S, Sweeney HL, Discher DE. Matrix elasticity directs stem cell lineage specification. *Cell*. 2006;126(4):677–689.
50. Fukada T, Hojyo S, Furuichi T. Zinc signal: a new player in osteobiology. *J Bone Miner Metab*. 2013;31(2):129–135.

International Journal of Nanomedicine

Publish your work in this journal

The International Journal of Nanomedicine is an international, peer-reviewed journal focusing on the application of nanotechnology in diagnostics, therapeutics, and drug delivery systems throughout the biomedical field. This journal is indexed on PubMed Central, MedLine, CAS, SciSearch®, Current Contents®/Clinical Medicine,

Submit your manuscript here: <http://www.dovepress.com/international-journal-of-nanomedicine-journal>

Dovepress

Journal Citation Reports/Science Edition, EMBase, Scopus and the Elsevier Bibliographic databases. The manuscript management system is completely online and includes a very quick and fair peer-review system, which is all easy to use. Visit <http://www.dovepress.com/testimonials.php> to read real quotes from published authors.